Deep ocean nutrients during the Last Glacial Maximum deduced from sponge silicon isotopic compositions

Katharine R. Hendry[1,2], R. Bastian Georg[2], Rosalind E.M. Rickaby[2], Laura F. Robinson[1] & Alex N. Halliday[2]

1. Department of Marine Chemistry and Geochemistry, Woods Hole Oceanographic Institution, Woods Hole, MA 02543, USA

2. Department of Earth Sciences, University of Oxford, Parks Road, Oxford OX1 3PR, UK.

Abstract

The relative importance of biological and physical processes within the Southern Ocean for the storage of carbon and atmospheric pCO_2 on glacial-interglacial timescales remains uncertain. Understanding the impact of surface biological production on carbon export in the past relies on the reconstruction of the nutrient supply from upwelling deep-waters. In particular, the upwelling of silicic acid ($Si(OH)_4$) is tightly coupled to carbon export in the Southern Ocean via diatom productivity. Here, we address how changes in deep-water $Si(OH)_4$ concentrations can be reconstructed using the silicon isotopic composition of deep-sea sponges. We report $\delta^{30}Si$ of modern deep-sea sponge spicules and show that they reflect seawater $Si(OH)_4$ concentration. The fractionation factor of sponge $\delta^{30}Si$ compared to seawater $\delta^{30}Si$ shows a positive relationship with $Si(OH)_4$, which may be a growth rate effect. Application of this proxy in two down-core records from the Scotia Sea reveals that $Si(OH)_4$ concentrations in the deep Southern Ocean during the Last Glacial Maximum (LGM) were no different than today. Our result does not support a coupling of carbon and nutrient build up in an isolated deep-ocean reservoir during

the LGM. Our data, combined with records of stable isotopes from diatoms, are only consistent with enhanced LGM Southern Ocean nutrient utilization if there was also a concurrent reduction in diatom silicification or a shift from siliceous to organic-walled phytoplankton.

Keywords: Porifera, spicule, silicic acid, deep-water, silicon cycle, glacial

1. Introduction

Debate still surrounds the relative importance of physical and biological mechanisms behind glacial-interglacial variations in atmospheric carbon dioxide (pCO_2; reviewed by Sigman and Boyle, 2000). The Southern Ocean has been implicated in the regulation of greenhouse gases through both types of mechanism. Firstly, a physical reduction in the ventilation of deep waters due to greater glacial sea-ice cover and ocean stratification, enhanced in a cooler ocean, would result in less outgassing of CO_2 to the atmosphere (e.g. de Boer et al., 2007). Secondly, an increase in biological export, accompanied by enhanced burial of carbon, would also reduce atmospheric pCO_2 during glacials (e.g. Kohfeld et al., 2005). A "biogeochemical divide" has been proposed, whereby biological export in the Antarctic Zone of the Southern Ocean regulates CO_2 directly, whereas export in the Subantarctic Zone controls global preformed nutrient supply, such that different regions around Antarctica may drive or respond to climate change by different mechanisms (Marinov et al., 2006). An understanding of Southern Ocean nutrients is clearly required to distinguish the physical and biological mechanisms that impact pCO_2 over glacial-interglacial timescales.

The concentration of silicic acid, $[Si(OH)_4]$, in deep-waters is governed by tectonics and silicate weathering on long timescales (>10^4 years) and by ocean productivity and ocean circulation on glacial-interglacial timescales (10^3-10^4 years; Ragueneau et al., 2000; Falkowski et al., 2004). As such the Si cycle is a synergistic driver of, and respondent to, the carbon (C) cycle and global climatic change. In the modern surface ocean, biological precipitation of amorphous silica (opal) by diatoms is the dominant process that removes

53 $Si(OH)_4$ from seawater, efficiently transporting silica and organic C to the seafloor. The
54 partitioning of C and Si between the surface and deep-ocean is controlled by the export and
55 remineralization of this biological material relative to vertical mixing rates (Toggweiler et
56 al., 1999; Ragueneau et al., 2000).

57 Diatom blooms rely on upwelling sources of $Si(OH)_4$ because efficient utilization
58 strips almost all of the Si from surface waters (Ragueneau et al., 2000). The nutrient
59 composition of upwelling waters, in particular the ratio of Si to other major nutrients, plays
60 a strong role in the population structure of phytoplankton growing in surface waters and
61 the biological pumping of C to deep-water (Yool and Tyrell, 2003; Falkowski et al., 2004).
62 Furthermore, reduced vertical mixing, or enhanced stratification, results in an increase in
63 deep-water C, and a corresponding reduction in atmospheric pCO_2. (Toggweiler, 1999).
64 Quantifying changes in the $Si(OH)_4$ content of deep-water is an important step towards
65 understanding the link between the sequestration of C, Si and other nutrients over glacial
66 cycles (Brzezinski et al., 2002; Matsumoto et al., 2002). The Southern Ocean is a key
67 location for studying paleo-$Si(OH)_4$ because of the regional and global importance of Si-
68 based productivity and its potential sensitivity to well documented proximal climatic
69 changes (Anderson et al., 2002).

70 The silicon isotopic composition ($\delta^{30}Si$) of biogenic opal provides a direct method
71 for quantifying seawater $Si(OH)_4$ budgets (de la Rocha et al., 1997; de la Rocha, 2003;
72 Beucher et al., 2007). Siliceous sponges (Phylum Porifera, Classes Demospongea and
73 Hexactinella) produce needle-like skeletal elements, spicules, composed of hydrated
74 amorphous silica. Uptake of ambient $Si(OH)_4$ occurs via a sodium transporter, which

resembles active transporters isolated from other metazoans (Schroeder et al., 2004). Biosilicification in sponges is controlled by two enzymes silicatein, which promotes condensation reactions, and silicase, which dissolves silica (Müller et al., 2007). A previously published study shows that the uptake of $Si(OH)_4$ results in fractionation of Si isotopes, such that spicules have some of the lightest $\delta^{30}Si$ signatures known in natural systems (de la Rocha, 2003). The $\delta^{30}Si$ of sponge spicules is a potential proxy to quantify whole ocean changes in Si cycling over timescales longer than the residence time of Si in the oceans (~15 ka), as well as changes in intermediate and deep-water $Si(OH)_4$ composition on shorter timescales (de la Rocha, 2003; de la Rocha and Bickle, 2005).

Here, we investigate the Si isotope composition of modern sponges and ambient waters from the Southern Ocean, and find a clear relationship between $[Si(OH)_4]$ and sponge spicule $\delta^{30}Si$ and Si isotope fractionation. We have then applied this calibration to sponge spicules picked from two cores in the Scotia Sea (Figure 1) to determine if $[Si(OH)_4]$ changed in response to the major climatic shifts since the Last Glacial Maximum (LGM).

2. Methods

2.1. Field setting and sample materials

The modern day Southern Ocean has large $[Si(OH)_4]$ gradients (Pollard et al., 2002) and an abundance of living sponges. Therefore, we have used a transect across the Drake Passage and Scotia Sea to undertake a calibration of sponge $\delta^{30}Si$ fractionation as a function of ambient $[Si(OH)_4]$. We focus our reconstruction of past $Si(OH)_4$ on the Scotia

96 Sea, which plays a disproportionately important role in global oceanography. It contains
97 both Antarctic and Subantarctic Zone waters, and acts as a bathymetric channel for the
98 Antarctic Circumpolar Current (ACC) and major oceanographic fronts. This flow results
99 in intense mixing and modification between the well ventilated and Si-rich Weddell Sea
100 derived deep-waters and the rest of the global oceans (Naveira Garabato et al., 2002). For
101 the calibration, we collected and analysed living specimens from a north-south transect
102 across the Scotia Sea and Drake Passage, encompassing a range of $[Si(OH)_4]$ (12 to 120
103 μM) and depths (300 to 2500 m; Figure 1A, 1B, Table 1). The $[Si(OH)_4]$ increases
104 polewards and with depth through a combination of water-mass mixing, remineralization
105 and an isopycnal gradient (Figure 1B; Pollard et al., 2002). Sponges were collected aboard
106 the *R/V Nathaniel B. Palmer* by either benthic trawl or dredge, and dried or frozen for
107 transit (April-May 2008). Water samples for $Si(OH)_4$ analysis were collected in niskin
108 bottles attached to deep-water CTD casts and a towed camera system (WHOI TowCam),
109 filtered immediately through 0.4 μm polycarbonate membranes (Whatman) and stored in
110 pre-cleaned HDPE bottles.

111 Additional samples were collected from coastal West Antarctic Peninsula (Figure 1)
112 and the North Atlantic. Core material was obtained from two cores in the Scotia Sea, from
113 south of the ACC (Piston core PC034, 1652m) and within the ACC (Kaston core KC081,
114 3662m; Figure 1; Table 2). All core material was sampled from the British Antarctic
115 Survey.

116 ## 2.2. Laboratory methods

117 The modern spicules were initially separated from organic matter by repeatedly heating
118 and sonicating in concentrated HNO_3 and H_2O_2 (Analar). Sediment grains were removed
119 by picking until visual inspection showed the spicules to be clear of detritus. The spicules
120 were then cleaned of any remaining organic matter and surface contaminants in a class 100
121 laboratory by heating in 50% quartz-distilled HNO_3/10% quartz-distilled HCl. Sediment
122 samples were deflocculated in sodium hexametaphosphate (5% w/v), sieved at 200 μm and
123 rinsed thoroughly in 18 MΩ.cm Milli-Q water. Approximately 20-30 spicules were hand
124 picked, rinsed with reagent grade methanol to remove clays, and heated with H_2O_2 to
125 remove organic matter.

126 The sponge spicules were then dissolved by heating in 0.2 M NaOH (Analar) at 100 ˚C for
127 3 days (Cardinal et al., 2007). The solution was then acidified to pH~2 using 0.2 N
128 thermally distilled HCl. Quantitative separation of Si from major ions was achieved using
129 a cation exchange resin (BioRad AG50W-X12; Georg et al., 2006), and diluted to 300-600
130 ppb Si depending on machine sensitivity.

131 The Si isotope analyses were carried out for Si isotopes ^{28}Si, ^{29}Si and ^{30}Si using the
132 *NuPlasma HR* MC-ICP-MS (University of Oxford) in medium resolution mode. The
133 samples were bracketed with a concentration-matched NBS28 standard (Georg et al., 2006,
134 2009; Reynolds et al., 2007), and isotope ratios calculated according to Equation 1.

135 $$\delta^{x}Si = \left(\left[\frac{R_{sam}}{R_{nbs28}} \right] - 1 \right) \times 1000 \qquad (1)$$

136 Each sample was measured 8 times on the mass spectrometer, and mean ratios calculated.
137 Standards were checked before every batch run to ensure accuracy (either "diatomite" with
138 $\delta^{30}Si$ = +1.26‰ (0.08), $\delta^{29}Si$= +0.65‰ (0.03) or "Big Batch" with $\delta^{30}Si$ = -10.67‰ (0.08),
139 $\delta^{29}Si$=-5.48‰ (0.05), parentheses indicating $2\sigma_{SE}=2\sigma_{SD}/\sqrt{n}$; Reynolds et al., 2007). Repeat
140 dissolutions, and repeat aliquots of the same dissolution, indicate an adequate level of
141 reproducibility comparable to previous studies (repeat measurements agree within
142 ~±0.15‰). Subsamples from the same modern sponge specimens were also analysed using
143 in-line gas fluorination followed by Isotope Ratio Mass Spectroscopy (IRMS; Finnigan
144 MAT 253) by M. Leng at the NERC Isotope Geosciences Laboratory (NIGL, Nottingham,
145 UK), yielding $\delta^{30}Si$ values within error of the measurements made at the University of
146 Oxford by MC-ICP-MS.

147 The $[Si(OH)_4]$ of water samples from the site of sponge collection were analysed at the
148 WHOI nutrient facility, and were consistent with Southern Ocean data from existing
149 databases (Schlitzer, 2000; Garcia et al., 2006). If there were no water samples collected in
150 the vicinity of the sponges, then $[Si(OH)_4]$ was estimated from existing data (Schlitzer,
151 2000; Garcia et al., 2006). For isotopic analysis, Si was quantitatively separated from
152 seawater using a modified Mg co-precipitation technique (Cardinal et al., 2005; Reynolds
153 et al., 2006). 2% by volume of 1M NaOH (Aristar) was added to 10-15 ml of seawater to
154 precipitate $Mg(OH)_2$, shaken, left for 1 hour, centrifuged and the supernatant transferred to
155 a new, clean tube. To ensure quantitative yields, the process was repeated twice adding
156 1% by volume NaOH to the supernatant each time. The precipitate was washed twice with
157 ~0.001M NaOH to remove anions, which can suppress intensity on the MC-ICP-MS. Ion

158 chromatography was used to show the precipitate wash effectively removed excess Cl^- and
159 F^- ions. The precipitate was then dissolved in 5% thermally distilled HNO_3 or HCl. The Si
160 was then purified using cation exchange as above; as before, matrix tests show the resin
161 effectively removes Na and other cations. The $\delta^{30}Si$ was measured using the same
162 protocol as for the spicules.

163 ## 3. Results and discussion

164 ### 3. 1. Modern calibration

165 Modern Southern Ocean sponge $\delta^{30}Si$ ranges from -0.70‰ to -4.13‰ (Figure 2A;
166 Table 3), in agreement with the limited published data from archived sponges (de la Rocha,
167 2003). A three isotope plot of all the silicon isotope data collected ($\delta^{29}Si$ vs. $\delta^{30}Si$) has a
168 slope of 0.51 (±0.01) calculated by model II regression (parentheses denotes the 95%
169 confidence interval), which is consistent with that anticipated for kinetic equilibrium
170 (0.509 or 0.511 depending on whether Si or SiO_2 undergoes fractionation; Reynolds et al.,
171 2007; Figure 2C). We find an inverse linear functional relationship between sponge $\delta^{30}Si$
172 and $[Si(OH)_4]$ (r^2= 0.75) according to Equation 2 (parentheses denotes the 95% confidence
173 interval, such that a single measurement of $\delta^{30}Si_{sponge}$ can give a $Si(OH)_4$ concentration to
174 approximately ±20 μM).

175 $$[Si(OH)_4] = -30.3(\pm 8.2)\delta^{30}Si_{sponge} - 13.79 \quad (2)$$

176 The measured seawater $\delta^{30}Si_{Si(OH)4}$ in the collected waters agree well with modeled (Table
177 4; Wischmeyer et al., 2003; Reynolds, 2009) and published data from other sectors of the

178 Southern Ocean (de la Rocha et al., 2000). Our $\delta^{30}Si_{Si(OH)4}$ values were used to calculate a
179 fractionation factor, ε (Equation 3; de la Rocha, 2003), which ranges from -2.5 to -5.3‰
180 and increases with ambient $Si(OH)_4$ (r^2=0.56; Figure 3A).

181 $$\varepsilon \approx \delta^{30}Si_{sponge} - \delta^{30}Si_{Si(OH)_4} \quad (3)$$

182 Subsamples from the same specimen, and of two co-existing specimens of the same
183 species, show $\delta^{30}Si$ is homogeneous within and between individuals bathed in the same
184 water mass (Figure 2B). We cannot rule out a ~0.5‰ species-specific offset in
185 fractionation, but it is small compared to the effect of environmental controls (~4‰; Figure
186 2A).

187 Other factors that are known to influence biomineralization co-vary with $[Si(OH)_4]$
188 in the Southern Ocean (e.g. temperature and pH; Foo et al., 2004). However, the samples
189 from coastal West Antarctic Peninsula and the deep North Atlantic show similar isotope
190 fractionations for a given $[Si(OH)_4]$ compared to sponges from the deep Southern Ocean
191 despite being collected under very different temperature, salinity and pH conditions
192 (Figure 3B-D). Consistent with growth under low $Si(OH)_4$ conditions, and in line with our
193 data, shallow-water sponges from a low nutrient tropical shelf show relatively heavy
194 isotopic compositions ($\delta^{30}Si_{sponge}$ from -2 to +0.5‰; Vroon et al., 2004). Our interpretation
195 that $[Si(OH)_4]$ is the dominant control over $\delta^{30}Si_{sponge}$ appears to hold in a variety of
196 oceanographic settings, providing a robust proxy for paleo-$[Si(OH)_4]$.

197 The environmental control over $\delta^{30}Si$ in sponges is likely to be a physiological
198 growth rate response to varying ambient $Si(OH)_4$ concentrations because ε is variable, and

199 correlates with $Si(OH)_4$ (Figure 3A). This control is not unexpected because silicification
200 is known to depend on $Si(OH)_4$ availability. Sponges produce different types of spicules
201 under Si limiting and replete conditions (Maldonado et al., 1999). Further, sponge culture
202 studies show there is a positive correlation between $Si(OH)_4$ availability and uptake rates,
203 and no apparent relationship with temperature (Frølich & Barthel, 1997). If the
204 fractionation process occurs at the site of Si uptake, greater uptake rates may lead to a
205 greater fractionation. Alternatively, $Si(OH)_4$ availability may control the internal
206 biochemical pathways involved during silicification, which may in turn determine isotopic
207 fractionation. For example, ambient $Si(OH)_4$ is a known modulating factor that regulates
208 the expression of silicatein and silicase, and induces expression of genes for other enzymes
209 involved in biosilicification (Perovic-Ottstadt et al., 2005; Müller et al., 2007). Further
210 work is required to understand the biosilicification process and, in particular, the reactions
211 that result in isotopic fractionation.

212 The Si isotope fractionation observed during the formation of sponge spicules is
213 greater than the fractionation observed during silicification of diatom opal (ε = -0.8 to -
214 2.1‰; Cardinal et al., 2005, 2007). Although diatoms use uptake transporters and
215 condensation/dissolution enzymes distinct to sponges, the mechanisms are somewhat
216 similar and may be homologous (Foo et al., 2004). However, we suggest the two groups
217 evolved Si acquisition mechanisms, which likely impact Si isotopes differentially, at
218 distinct points in Earth history. Siliceous sponges originated in the Precambrian (Love et
219 al,. 2009), with a relatively low affinity for Si (Frølich & Barthel, 1997), at a time when
220 weathering of silicate rocks resulted in high oceanic $Si(OH)_4$ (Siever, 1992). In contrast,

diatoms evolved in the Jurassic (Sims et al., 2006) with a higher affinity for Si, probably because biological utilization by other siliceous organisms resulted in lower oceanic $Si(OH)_4$ (Maldonado et al., 1999).

3.2. Downcore data

We use the modern relationship between $[Si(OH)_4]$ and $\delta^{30}Si_{sponge}$, and analyses of spicules hand-picked from two Scotia Sea sediment cores, to investigate whether deep-water $[Si(OH)_4]$ changed within the ACC on glacial-interglacial timescales, and to address the potential consequences for atmospheric pCO_2 levels in the past.

Our modern core-top sample from piston core PC034 (Figure 4A; $\delta^{30}Si_{sponge}$ = -3.86±0.17‰, $\pm 2\sigma_{SD}$) agrees well with the living sponges collected from the southern Scotia Sea, growing in $[Si(OH)_4]$ of approximately 100 μM (Figure 2A, 4B). The youngest section of the northern site (KC081) has been dated at ~6 ka (Figure 4A), so we are unable to measure a core-top sample at the site. In both cores, the Last Glacial Maximum (LGM) value is similar to the modern, suggesting deep-water $[Si(OH)_4]$ was not significantly different at the LGM compared to today at either site (within ~20 μM). The similarity between LGM and modern $[Si(OH)_4]$ in Southern Ocean deep-waters provides insight into processes occurring in different regions of the water column on glacial-interglacial timescales.

The fractionation factor, ε, would be the most appropriate parameter to record because it would account for changes in seawater $\delta^{30}Si_{Si(OH)4}$. However, $\delta^{30}Si_{Si(OH)4}$ of seawater cannot be constrained directly downcore, and so here we present $\delta^{30}Si_{sponge}$ and

assume that $\delta^{30}Si_{Si(OH)4}$ of deep waters is constant over glacial-interglacial cycles in accord with recent box modeling (Georg et al., 2009).

There are two important caveats when interpreting our downcore data. Firstly, age models for cores in the Southern Ocean are notoriously challenging due to poor preservation of benthic foraminifera and other dateable carbonates. Here, we apply the best dating constraints available, based on radiocarbon measurements and stratigraphic markers, locating the LGM using the abundance of diatoms and the radiolarian *Cycladophora davisiana* (Figure 4A). The limited number of tie-points results in an inherent degree of uncertainty on the age model. Secondly, as is a common problem with any sedimentary proxy, there is a possibility that core components, such as spicules, undergo differential transport and are of different ages to surrounding grains. However, sponges are benthic and, in life, comprise a large proportion of sticky organic matter, making significant post-mortem transportation of spicules less likely than, for example, planktonic diatoms or foraminifera. Opal-specific dating methods may resolve any issues arising from particulate transportation (Ingalls et al., 2004).

3.2.1. Deep processes: the glacial carbon reservoir

A leading hypothesis for the reduced pCO_2 during the glacial is the presence of an isolated reservoir of C-rich water in the Pacific and Southern Oceans (Marchitto and Broecker 2006; Marchitto et al., 2007). Radiocarbon records from Baja California and the Equatorial Pacific point towards a deglacial degassing of old C from a reservoir isolated during the LGM (Marchitto et al., 2007; Stott et al., 2009). Deglacial age deep-sea corals

263 from the Drake Passage, dated to Heinrich Event 1 (~16.7 ka), also show radiocarbon
264 depletion, but not to such a great extent as the Baja California record (Robinson & van de
265 Flierdt, 2009). Benthic foraminiferal records from the Southern Ocean show very light
266 $\delta^{13}C$ signatures, indicative of a high nutrient content or significant changes in air-sea
267 exchange of inorganic C (Curry et al., 1998; Marchitto and Broecker, 2006; Marchitto et
268 al., 2007). Specifically, there is evidence for a strong vertical $\delta^{13}C$ gradient at
269 approximately 2.5km to the north of the polar front in the South Atlantic during the glacial
270 (Hodell et al., 2003). However, records of benthic foraminiferal Cd/Ca, a proxy for
271 dissolved phosphate (P), do not support a significant change between the nutrient content
272 of the modern and LGM deep Southern Ocean (Boyle, 1992). This discrepancy has led to
273 considerable debate in the paleoceanographic community surrounding the continued
274 presence of nutrient-poor North Atlantic derived waters in the ACC. One possibility,
275 consistent with a continued presence of NADW in the Glacial Southern Ocean, is that the
276 light $\delta^{13}C$ was associated either with changes in air-sea exchange of C (Broecker, 1993;
277 Lynch-Stieglitz & Fairbanks, 1994; Marchitto & Broecker, 2006) or organic matter with
278 high C:P content (Arrigo, 1999; Elderfield & Rickaby, 2000). Alternatively, several
279 studies have highlighted caveats and artifacts associated with both $\delta^{13}C$ in regions of high
280 organic matter accumulation rate (Mackensen et al., 1993) and Cd/Ca where significant
281 dissolution has occurred (McCorkle et al., 1995). When outliers in Southern Ocean
282 datasets of individual foraminiferal shells of a single benthic species, potentially arising
283 from changes in productivity in high organic accumulation rate regions, are removed the
284 resulting "representative" $\delta^{13}C$ brings $\delta^{13}C$ more inline with Cd/Ca. These data, together

285 with $^{231}Pa/^{230}Th$ records of water mass export (Yu et al,. 1996), are consistent Glacial
286 NADW entering the ACC followed by transportation to the North Pacific in a similar
287 fashion to the modern ocean (Matsumoto & Lynch-Stieglitz, 1999).

288 Our $\delta^{30}Si$ results from KC081, situated greater than 3km, below the glacial $\delta^{13}C$ gradient,
289 (Hodell et al., 2003), do not show a change between the modern and the LGM, so we infer
290 that, any isotopically light C in the deep Southern Ocean was not associated with higher
291 levels of $Si(OH)_4$. Furthermore, our results are consistent with the benthic foraminiferal
292 Cd/Ca records, suggesting there were insignificant changes in both refractory and labile
293 nutrient concentrations in Southern Ocean deep-waters during the LGM. In this case, the
294 light $\delta^{13}C$ signature of the LGM Southern Ocean could have been caused by a reduction in
295 air-sea exchange of inorganic C (CO_2) due to poor ventilation, or changes in the surface
296 temperature or residence time of subducting deep waters (e.g. Broecker, 1993; Lynch-
297 Stieglitz & Fairbanks, 1994; Mackensen, 2001). For example, the isolation of a deep-
298 water mass, due to stratification or sea-ice cover, could lead to a depletion in $\delta^{13}C$ and a
299 decrease in atmospheric CO_2 without a concurrent change in nutrients (Toggweiler, 1999).

300 Alternatively, the light $\delta^{13}C$ could originate from the remineralization of organic C
301 that is not associated with significant quantities of $Si(OH)_4$ or P. This decoupling could be
302 a result of physiological changes within the diatom populations, or shifts in the
303 phytoplankton population structure, during the LGM. Firstly, extensive field and
304 laboratory experiments have shown that diatoms have both lower cellular Si:N and P:N
305 when grown under Fe replete conditions than when Fe stressed or limited (Timmermans et
306 al., 2004; Brzezinksi et al., 2005; Price, 2005). The higher Fe conditions existing in the

307 Southern Ocean during glacials, due to enhanced dust supply (e.g. Kohfeld et al., 2005),
308 are thought to promote lower Si:N uptake ratios in diatoms compared to Fe-stressed
309 diatoms growing during interglacials (Brzezinksi et al., 2002). Secondly, the non-siliceous
310 dinoflagellate *Phaeocystis* shows a high N:P uptake ratio during modern Southern Ocean
311 blooms. If *Phaeocystis* blooms became more dominant in stratified waters during the LGM
312 (Arrigo, 1999; Elderfield and Rickaby 2000), then export of the associated organic C, and
313 subsequent remineralization in deep-waters, could result in a depletion in $\delta^{13}C$ and an
314 increase in NO_3 without a concurrent increase in either $Si(OH)_4$ or P. These two scenarios
315 are not mutually exclusive, and both may have contributed to the nutrient conditions
316 prevailing in the glacial Southern Ocean.

317 3.2.2. Surface processes: glacial nutrient utilization

318 In addition to the deep-water signal, our results provide further information about
319 biological utilization in surface waters at the LGM. The Silicic Acid Leakage Hypothesis
320 (SALH) proposes that reduced productivity, due the physiological response of
321 phytoplankton to Fe fertilization, caused a reduction in the Si to N uptake ratio in the
322 Southern Ocean during the LGM (Brzezinski et al., 2002; Matsumoto et al., 2002).
323 According to the SALH, a pool of excess $Si(OH)_4$ in Antarctic surface waters was exported
324 to lower latitudes, via intermediate water, promoting diatom production at the expense of
325 carbonate-producing coccolithophores. In this scenario, there would be an increase in
326 export of organic C with respect to inorganic C in the low latitudes associated with a rise in
327 ocean alkalinity and lowered atmospheric pCO_2 (Brzezinski et al., 2002; Matsumoto et al.,
328 2002). Diatom $\delta^{30}Si$ records show a 0.5‰ change across the deglaciation, which have

329 been interpreted as a reduction in the fraction of $Si(OH)_4$ utilized in the Antarctic (de la
330 Rocha et al., 1997), subantarctic and subtropics during the LGM (Beucher et al., 2007).
331 Since whole ocean $\delta^{30}Si$ changes are unlikely over this timescale (Georg et al., 2009), our
332 new record demonstrates that the decrease in $Si(OH)_4$ surface depletion in the subantarctic
333 region (Beucher et al., 2007) was not caused by changes in the $[Si(OH)_4]$ concentration of
334 upwelling waters (Figure 4B). Instead it must have been a consequence of either an
335 increase in upwelling intensity or reduced surface utilization. We argue above that the
336 geochemical evidence points towards an increase in stratification in the ACC south of the
337 polar front during the LGM, so the diatom $\delta^{30}Si$ data is best explained by changes in the
338 efficiency of surface utilization (Beucher et al., 2007). Records of nitrogen isotopes ($\delta^{15}N$)
339 of diatom-bound organic matter indicate an increase in utilization of nitrate in surface
340 waters (Sigman et al., 1999; Robinson et al., 2004). This can be reconciled with the
341 diatom $\delta^{30}Si$ data if there was a large-scale physiological change in diatoms reducing Si:N
342 and P:N uptake ratios (e.g. Brzezinksi et al,. 2005), or an increase in productivity by non-
343 siliceous phytoplankton, such as *Phaeocystis* (Arrigo, 1999; Elderfield and Rickaby, 2000).

344 ### 3.2.3. Implications for glacial pCO_2

345 Our new sponge $\delta^{30}Si$ data, when combined with other geochemical proxies, bring
346 new insight into the mechanisms behind the lower glacial atmospheric pCO_2. Deep-water
347 C and macronutrients are decoupled on glacial-interglacial timescales as a result of
348 physical processes, such as ocean stratification or sea-ice cover, which lock-up C in the
349 deep ocean and lower atmospheric pCO_2 (Toggweiler, 1999; Stephens and Keeling, 2000).

350 An increase in the biological export of C from the surface to the deep ocean is consistent
351 with all of the currently available data if there was either a concurrent decrease in diatom
352 silicification, or a shift away from siliceous to organic-walled phytoplankton production, in
353 the Southern Ocean. Whilst this could increase the C:Si and C:P content of the deep
354 ocean, without significant mineral ballast a lightly-silicified diatom or *Phaeocystis*
355 dominated biological pump would not export as C efficiently as one dominated by heavily-
356 silicified diatoms (Jin et al., 2006), limiting the impact on atmospheric pCO_2. However,
357 the excess $Si(OH)_s$ resulting from a decrease in surface utilization in the Southern Ocean
358 could have been exported away from the subantarctic via mode waters without impacting
359 the deep-water Si inventory. This would have the potential to impact atmospheric pCO_2 by
360 increasing the relative productivity of diatoms in the lower latitudes (Matsumoto et al.,
361 2002; Bradtmiller et al., 2007).

362 3.2.4. The deglaciation

363 During the deglacial (after ~ 18 kyr), our records indicate a depletion in deep-water
364 $[Si(OH)_4]$ both within and south of the ACC (Figure 4B). In the late Holocene, deep-water
365 $[Si(OH)_4]$ recovers to modern values. Given the uncertainty on the age models, we cannot
366 pin point the exact timing of these changes but the decline is a robust observation in both
367 cores. Our best estimate for the maximum rate of change of deep-water $[Si(OH)_4]$ is
368 approximately 10 $\mu M\ ky^{-1}$

369 We hypothesize two possible mechanisms behind this decline in deep-water
370 Si(OH)4: large scale changes in nutrients arising from decomposition of biogenic particles

371 in the deep Southern Ocean ("remineralized nutrients") or localized changes in unutilized
372 nutrients subducted during deep-water formation ("preformed nutrients"; Marinov et al.,
373 2006). Firstly, our data are consistent with storage of $Si(OH)_4$ in the form of a large-scale
374 opal deposition in the Southern Ocean during the deglacial (10-16 kyr), caused by wind-
375 driven upwelling of water enriched in $Si(OH)_4$ relative to the surface. Enhanced opal
376 fluxes during the deglaciation, coupled with $^{231}Pa/^{230}Th$ activity ratios, have been observed
377 in Pacific and Atlantic Sectors of the Southern Ocean and equatorial regions (Anderson et
378 al., 2009). Such a significant and widespread burial of opal could have resulted in a drop in
379 deep ACC remineralized $Si(OH)_4$, whilst the enhanced upwelling drove a concurrent rise
380 in pCO_2 (Anderson et al., 2009). The decline in deep-water $[Si(OH)_4]$ would have led to a
381 negative feedback, by limiting the amount of productivity that could be supported by
382 upwelling water and an eventual restoration of export production rates, opal fluxes and
383 $[Si(OH)_4]$ gradients over time. Such changes in remineralized nutrients cannot change
384 global deep-water $[Si(OH)_4]$ over timescales of less than the residence time of Si in the
385 whole ocean (~15 ky; Georg et al., 2009). However, we constructed a simple one-box
386 model for the deep Southern Ocean alone (south of 50°S, > 400 m depth, area ~ 25×10^{12}
387 m^2), using a mean modern $[Si(OH)_4]$ of 100 μM and mean depth of 4000 m (Garcia et al.,
388 2006), and modern opal accumulation fluxes of ~ 0.2 mol Si m^{-2} yr^{-1} (Pondaven et al.,
389 2000). Using this model, we estimate changes in the opal burial rate relative to Si inputs of
390 ~ 20% (less than observed in core TN057-13-4PC; Figure 4b, Anderson et al., 2009) could
391 cause changes of the order of 10 μM in 1000 years, which are sufficient to explain our
392 observations.

393 Alternatively, the rapid rates in change indicate the decline in deep-water [$Si(OH)_4$]
394 during the deglaciation was at least in part a result of localized inputs of preformed
395 nutrients. For example, the retreat of the Weddell Sea ice shelf during the deglacial and
396 early Holocene "Hypsithermal" may have changed deep-water formation processes and led
397 to a decline in the input of highly Si-enriched Weddell Sea Deep Water (WSDW) into the
398 ACC (Yoon et al., 2007). This could explain both the rapid decline in deep-water $Si(OH)_4$
399 and the apparent divergence in the records between ~ 6-10 ky (higher [$Si(OH)_4$] from the
400 southern core compared to the northern core; Figure 4B). Resumption of WSDW input to
401 the ACC could be in part responsible for the recovery in deep-water $Si(OH)_4$ in the later
402 Holocene. Future research should focus on constraining this climatically important time,
403 in order to understand the response of Southern Ocean deep-water circulation during
404 periods of global warming.

405 ## 4. Summary and conclusions

406 In summary, we show the potential for combined $\delta^{30}Si$ records from diatoms and
407 sponges to constrain the surface and deep components of the Si biological pump. We
408 investigate fractionation by modern deep-sea sponges, and find the $\delta^{30}Si$ of spicules and
409 fractionation with respect to ambient seawater correlate with the ambient [$Si(OH)_4$]. We
410 then apply this calibration to two downcore records from the Scotia Sea. Our results show
411 that the deep-waters of the LGM Southern Ocean were not enriched in $Si(OH)_4$, suggesting
412 that the isolated reservoir of old, isotopically depleted C was not associated with an
413 increase in either $Si(OH)_4$ or P. Instead, the Southern Ocean resulted in lower atmospheric
414 pCO_2 during the glacial largely due to reduction in air-sea exchange of C via a physical

process. If there was an enhanced glacial biological pump in the Southern Ocean, it was likely to have been dominated by lightly-silicified diatoms or organic-walled phytoplankton (e.g *Phaeocystis*) resulting in a concurrent increase in surface nitrate utilization, and a change in deep-water nutrient ratios that may not have been associated with a considerable increase in pump efficiency. Utilization of Si-rich upwelling waters by diatoms was lower during the LGM, providing a surplus of $Si(OH)_4$ that could then be exported to lower latitudes via intermediate waters, where enhanced export production could lower atmospheric CO_2. During the deglaciation, there is a robust and significant decrease in deep-water $Si(OH)_4$, which could be associated with a pulse of opal burial linked with wind-driven upwelling and concurrent rise in pCO_2, or a change in water mass inputs.

References

Anderson, R.F., Chase, Z., Fleisher, M.Q., Sachs, J., 2002. The Southern Ocean's biological pump during the Last Glacial Maximum. Deep-Sea Res. II. 49, 1909-1938.

Anderson, R.F., Ali, S., Bradtmiller, L.I., Nielsen, S.H.H., Fleisher, M.Q., Anderson, B.E., Burckle, L.H., 2009. Wind-driven upwelling in the Southern Ocean and the deglacial rise in atmospheric CO2. Science. 323, 1443-1448.

Arrigo, K., 1999. Phytoplankton community structure and the drawdown of nutrients and CO_2 in the Southern Ocean. Science. 283, 365-367.

Beucher, C.P., Brzezinksi, M.A., Crosta, X., 2007. Silicic acid dynamics in the glacial sub-Antarctic: Implications for the silicic acid leakage hypothesis. Global Biogeochem. Cycles. 21, doi:10.1029/2006GB002746.

Boyle, E., 1992. Oceanic chemical distributions during stage 2 glacial maximum: cadmium and d13C evidence compared. Ann. Rev. Earth and Planet. Sci. 20, 245-287.

Bradtmiller, L.I., Anderson, R.F., Fleisher, M.Q., Burckle, L.H., 2007. Opal burial in the equatorial Atlantic Ocean over the last 30 ka: implicatons for glacial-interglacial changes in the ocean silicon cycle. Paleoceanography. 22, doi:10.1029/2007PA001443.

Broecker, W.S., 1993. An oceanographic explanation for the apparent carbon isotope-

cadmium discordancy in the glacial Antarctic? Paleoceanography. 8, 137-139.
Brzezinski, M.A., Sigman, D.M., Sarmiento, J.L., Matsumoto, K., Gruber, N., Rau, G.H., Coale, K.H., 2002. A switch from $Si(OH)_4$ to NO_3^- depletion in the glacial Southern Ocean. Geophys. Res. Lett. 29, 1564.
Brzezinksi, M.A., Jones, J.L., Demarest, M.S., 2005. Control of silica prodcution by iron and silicic acid during the Southern Ocean Iron Experiment (SOFeX). Limnology & Oceanography. 50, 810-824.
Cardinal, D., Alleman, L.Y., Dehairs, F., Savoye, N., Trull, T.W., Andre, L., 2005. Relevance of silicon isotopes to Si-nutrient utilization and Si-source assessment in Antarctic waters. Global Biogeochemical Cycles. 19, doi:10.1029/2004GB002364.
Cardinal, D., Savoye, N., Trull, T.W., Dehairs, F., E.E., K., Fripiat, F., Tison, J.-L., André, L., 2007. Silicon isotope in spring Southern Ocean diatoms: large zonal changes despite homogeneity among size fractions. Mar. Chem. 106, 46-62.
de Boer, A.M., Sigman, D.M., Toggweiler, J.R., Russell, J.L., 2007. Effect of global ocean temperature change on deep ocean ventilation. Paleoceanography. 22, PA2210, doi:2210.1029/2005PA1242.
de la Rocha, C., Brzezinksi, M.A., DeNiro, M.J., 1997. Fractionation of silicon isotopes by marine diatoms during biogenic silica formation. Geochim. Cosmochim. Acta 61, 5051-5056.
de la Rocha, C.L., Brzezinksi, M.A., DeNiro, M.J., 2000. A first look at the distribution of the stable isotopes of silicon in natural waters. Geochim. Cosmochim. Acta. 64, 2467-2477.
de la Rocha, C.L., 2003. Silicon isotope fractionation by marine sponges and the reconstruction of the silicon isotope composition of ancient deep water. Geology. 31, 423-426.
de la Rocha, C., Bickle, M., 2005. Sensitivity of silicon isotopes to whole-ocean changes in the silica cycle. Mar. Geol. 217, 267-282.
Elderfield, H., Rickaby, R., 2000. Oceanic Cd/P ratio and nutrient utilization in the glacial Southern Ocean Nature. 405, 305-310.
Falkowski, P.G., Katz, M.E., Knoll, A.H., Quigg, A., Raven, J.A., Schofield, O., Taylor, F.J.R., 2004. The evolution of modern eukaryotic phytoplankton. Science. 305, 354-360.
Fluckiger, J., Dallenbach, A., Blunier, T., Stauffer, B., Stocker, T.F., Raynaud, D., Barnola, J.M., 1999. Variations in atmospheric N_2O concentration during abrypt climatic changes. Science. 285, 227-230.
Foo, C.W.P., Huang, J., Kaplan, D.L., 2004. Lessons from seashells: silica mineralization via protein templating. Trends Biotechnol. 22, 577-585.
Frøhlich, H., Barthel, D., 1997. Silica uptake of the marine sponge Halichondria panicea in Kiel Bight. Mar. Biol. 128, 115-125.
Garcia, H.E., R.A. Locarnini, T.P. Boyer, and J.I. Antonov. World Ocean Atlas 2005, volume 4: Nutrients (phosphate, nitrate, silicate). S.Levitus, Ed. NOAA Atlas NESDIS 64, U.S. Government Printing Office, Washington, D.C., 396pp (2006).
Georg, R.B., Reynolds, B.C., Frank, M., Halliday, A.N., 2006. New sample preparation techniques for the determination of Si isotopic composition using MC-ICPMS. Chem. Geol. 235, 95-104.

491 Georg, R.B., West, A.J., Basu, A.R., Halliday, A.N., 2009. Silicon fluxes and isotope
492 composition of direct groundwater discharge into the Bay of Bengal and the effect
493 on the global ocean silicon budget. Earth and Planetary Science Letters. 283, 67-74.
494 Hodell, D.A., Venz, K.A., Charles, C.D., Ninnemann, U.S., 2003. Pleistocene vertical
495 carbon isotope and carbonate gradients in the South Atlantic sector of the Southern
496 Ocean. Geochemistry Geophysics Geosystems. 4, 1004;
497 doi:1010.1029/2002GC000367.
498 Indermühle, A., Stocker, T.F., Joos, F., Fischer, H., Smith, H.J., Wahlen, M., Deck, B.,
499 Mastroianni, D., Tschumi, J., Blunier, T., Meyer, R., Stauffer, B., 1999. Holocene
500 carbon-cycle dynamics based on CO_2 trapped in ice at Taylor Dome. Nature. 398,
501 121-126.
502 Ingalls, A.E., Anderson, R.F., Pearson, A., 2004. Radiocarbon dating of diatom-bound
503 organic compounds. Marine Chemistry. 92, 91-105.
504 Jin, X., Gruber, N., Dunne, J.P., Sarmiento, J.L., Armstrong, R.A., 2006. Diagnosing the
505 contribution of phytoplankton functional groups to the production and export of
506 particulate organic carbon, $CaCO_3$, and opal from global nutrient and alkalinity
507 distributions. Global Biogeochemical Cycles. 20, doi:10.1029/2005GB002532.
508 Kohfeld, K.E., Le Quere, C., Harrison, S.P., Anderson, R.F., 2005. Role of marine biology
509 in glacial-interglacial CO_2 cycles. Science. 308, 74-78.
510 Love, G.D., Grosjean, E., Stalvies, C., Fike, D.A., Grotzinger, J.P., Bradley, A.S., Kelly,
511 A.E., Bhatia, M., Meredith, W., Snape, C.E., Bowring, S.A., Condon, D.J.,
512 Summons, R.E., 2009. Fossil steroids record the appearance of Demospongiae
513 during the Cryogenian period. Nature. 457, 718-722.
514 Lynch-Stieglitz, J., Fairbanks, R.G., 1994. A conservative tracer for glacial ocean
515 circulation from carbon isotope and palaeo-nutrient measurements in benthic
516 foraminifera. Nature. 369, 308-310.
517 Mackensen, A., 2001. Oxygen and carbon stable isotope traces of Weddell Sea water
518 masses: new data and some paleoceanographic implications. Deep-Sea Res. I. 48,
519 1401-1422.
520 Maldonado, M., Carmona, M.C., Uriz, M.J., Cruzado, A., 1999. Decline in Mesozoic reef-
521 building sponges explained by silicon limitation. Nature. 401, 785-788.
522 Marchitto, T.M., Broecker, W.S., 2006. Deep water mass geometry in the glacial Atlantic
523 Ocean: a review of constraints from the paleonutrient proxy Cd/Ca. Geochem.
524 Geophys. Geosyst. 7, Q12003, doi:12010.11029/12006GC001323.
525 Marchitto, T.M., Lehman, S.J., Ortiz, J.D., Fluckiger, J., van Geen, A., 2007. Marine
526 radiocarbon evidence for the mechanism of deglacial atmospheric CO_2 rise.
527 Science. 316, 1456-1460.
528 Marinov, I., Gnanadesikan, A., Toggweiler, R., Sarmiento, J.L., 2006. The Southern Ocean
529 biogeochemical divide. Nature. 441, 964-968.
530 Matsumoto, K., Lynch-Stieglitz, J., 1999. Similar glacial and Holocene deep water
531 circulation inferred fro southeast Pacific benthic foraminiferal carbon isotope
532 composition. Paleoceanography. 149-163.
533 Matsumoto, K., Sarmiento, J.L., Brzezinksi, M.A., 2002. Silicic acid leakage from the
534 Southern Ocean: a possible explanation for glacial atmospheric pCO2. Global
535 Biogeochemical Cycles. 16, 1031.

536 McCorkle, D.C., Martin, P.A., Lea, D.W., Klinkhammer, G.P., 1995. Evidence of a
537 dissolution effect on benthic foraminiferal shell chemistry - $\delta^{13}C$, Cd/Ca, Ba/Ca and
538 Sr/Ca: results from t Ontong Java Plateau. Paleoceanography. 10, 699-714.
539 Monnin, E., Indermuhle, A., Dallenbach, A., Fluckieger, J., Stauffer, B., Stocker, T.F.,
540 Raynaud, D., Barnola, J.M., 2001. Atmospheric CO_2 concentrations over the Last
541 Glacial Termination. Science. 291, 112-114.
542 Monnin, E., Steig, E.J., Siegenthaler, U., Kawamura, K., Schwander, J., Stauffer, B.,
543 Stocker, T., Morse, D.L., Barnola, J.-M., Bellier, B., Raynaud, D., Fischer, H.,
544 2004. Evidence for substation accumulation rate variability in Antarctica during the
545 Holocene, through synchronization of CO_2 in the Taylor Dome, Dome C and DML
546 ice cores Earth Planet. Sci. Letts. 224, 45-54, doi:10.1016/j.epsl.2004.1005.1007.
547 Müller, W.E.G., Li, J., Schroeder, H.C., Qiao, L., Wang, X., 2007. The unique skeleton of
548 siliceous sponges (Porifera; Hexactinellida and Demospongiae) that evolved first
549 from the Urmetazoa during the Proterozoic: a review. Biogeosciences. 4, 219-232.
550 Naveira Garabato, A.C., Heywood, K.J., Stevens, D.P., 2002. Modification and pathways
551 of Southern Ocean deep waters in the Scotia Sea. Deep-Sea Res. I. 49, 681-705.
552 Perovic-Ottstadt, S., Wiens, M., Schroeder, H.C., Batel, R., Giovine, M., Krasko, A.,
553 Müller, I.M., Müller, W.E.G., 2005. Arginine kinase in the demosponde Suberites
554 domuncula: regulation of its expression and catalytica activity by silicic acid. J.
555 Exp. Biol. 208, 637-646.
556 Pollard, R.T., Lucas, M.I., Read, J.F., 2002. Physical controls on biogeochemical zonation
557 in the Southern Ocean. Deep-Sea Res. II. 49, 3289-3305.
558 Pondaven, P., Ragueneau, O., Tréguer, P., Hauvespre, A., Dezileau, L., Reyss, J.L., 2000.
559 Resolving the "opal paradox" in the Southern Ocean. Nature. 405, 168-172.
560 Price, N.M., 2005. The elemental stoichiometry and composition of an iron-limited diatom.
561 Limnology and Oceanography. 50, 1159-1171.
562 Ragueneau, O., Tréguer, P., Leynaert, A., Anderson, R.F., Brzezinksi, M.A., DeMaster,
563 D.J., Dugdale, R.C., Dymond, J., Fischer, G., Francois, R., Heinze, C., Maier-
564 Raimer, E., Martin-Jezequel, V., Nelson, D.M., Quéguiner, B., 2000. A review of
565 the Si cycle in the modern ocean: recent progress and missing gaps in the
566 application of biogenic opal as a paleoproductivity proxy. Global Planet. Change.
567 26, 317-365.
568 Reynolds, B.C., Frank, M., Halliday, A.N., 2006. Silicon fractionation during nutrient
569 utilization in the North Pacific. Earth Planet. Sci. Letts. 244, 431-443.
570 Reynolds, B.C., Aggarwal, J., Andre, L., Baxter, D., Beucher, C., Brzezinksi, M.A.,
571 Engstrom, E., Georg, R.B., Land, M., Leng, M.J., Opfergelt, S., Rodushkin, I.,
572 Sloane, H.J., van der Boorn, S.H.J.M., Vroon, P.Z., Cardinal, D., 2007. An inter-
573 laboratory comparison of Si isotope reference materials. J. Anal. Atom. Spectrom.
574 22, 561-568.
575 Reynolds, B.C., 2009. Modeling the modern marine d30Si distribution. Global
576 Biogeochem. Cycles. 23, GB2015, doi:2010.1029/2008GB003266.
577 Robinson, R.S., Brunelle, B.G., Sigman, D.M., 2004. Revisiting nutrient utilization in the
578 glacial Antarctic: evidence from a new method for diatom-bound N isotope
579 analysis. Paleoceanography. 19, doi:10.1029/2003PA000996.
580 Robinson, L.F., van de Flierdt, T., 2009. Southern Ocean evidence for reduced export of

North Atlantic Deep Water during Heinrich event 1. Geology. 37, 195-198.
Schlitzer, R., Applying the adjoint method for global biogeochemical modelling, Inverse methods in global biogeochemical modelling 114, AGU Geophys. Monogr. Ser. 114, 1999.
Siever, R., 1992. The silica cycle in the Precambrian. Geochim. Cosmochim. Acta. 56, 3265-3272.
Sigman, D.M., Altabet, M.A., Francois, R., MCCorkle, D.C., Gaillard, J.-F., 1999. The isotopic composition of diatom-bound nitrogen in Southern Ocean sediments Paleoceanography. 14, 118-134.
Sigman, D.M., Boyle, E.A., 2000. Glacial/interglacial variations in atmospheric carbon dioxide. Nature. 407, 859-869.
Sims, P.A., Mann, D.G., Medlin, L.K., 2006. Evolution of diatoms: insights from fossil, biological and molecular data. Phycologia. 45, 361-402.
Stephens, B.B., Keeling, R.F., 2000. The influence of Antarctic sea-ice on glacial-interglacial CO_2 variations. Nature. 404, 171-174.
Stott, L., Southon, J., Timmerman, A., Koutavas, A., 2009. Radiocarbon age anomaly at intermediate water depth in the Pacific Ocean during the last deglaciation. Paleoceanography. 24, PA2223, doi:2210.1029/2008PA001690.
Timmermans, K.R., van der Wagt, B., de Baar, H.J.W., 2004. Growth rates, half-saturation constants, and silicate, nitrate, and phosphate depletion in relations to iron availability of four large, open-ocean diatoms from the Southern Ocean. Limnology and Oceanography. 49, 211-2151.
Toggweiler, R., 1999. Variation of atmospheric CO_2 by ventilation of the ocean's deepest water. Paleoceanography. 14, 571-588.
Vroon, P.Z., Beets, K.J., Soenardo, D.H., van Soest, R.W., Trolestra, S.R., Schwieters, J., van Belle, C.C., van der Wagt, B., 2004. Fractionation of silicon isotopes by present-day demosponges from the Spermonde Shelf, Indonesia. Eos. Trans. AGU. 85(47), Abstract V54B-02.
Wischmeyer, A.G., de la Rocha, C., Maier-Raimer, E., Wolf-Gladrow, D.A., 2003. Control mechanisms for the oceanic distribution of silicon isotopes. Global Biogeochem. Cycles. 17, doi:10.1029/2002GB002022.
Yool, A., Tyrrell, T., 2003. Role of diatoms in regulating the ocean's silicon cycle. Global Biogeochem. Cycles. 17, Art no. GB002018.
Yoon, H.-I., Khim, B.K., Yoo, K.-C., Bak, Y.S., Lee, J.I., 2007. Late glacial to Holocene climatic and oceanographic record of sediment facies from the South Scotia Sea off the northern Antarctic Peninsula. Deep-Sea Research II. 54, 2367-2387.
Yu, E.-F., Francois, R., Bacon, M., 1996. Similar rates of modern and last-glacial Ocean thermohaline circulation inferred from radiochemical data. Nature. 379, 689-694.

The authors would like to thank the captain and crew of the *R/V Nathaniel B. Palmer* (cruise NBP0805; Program Manager Thomas Wagner). Thanks also to Rhian Waller (University of Hawaii), Laura Schejter

(INIDEP, Argentina), Jade Berman (University of Victoria, Wellington), Nicky White (University of Cambridge) and Andy Clarke (British Antarctic Survey) for sponge samples and help with identification. Thanks to Chris Siebert, Helen Williams, Sune Nielsen, Ros Armytage and Paul Savage (University of Oxford) for assistance in the laboratory, Melanie Leng (NIGL) for additional silicon isotope measurements, Maureen Auro and Paul Henderon (WHOI) for assistance with nutrient analyses and Kathy Scanlon (USGS) for map production. Core material and age model from Claire Allen and Claus-Dieter Hillenbrand (British Antarctic Survey). Thanks to Louisa Bradtmiller (WHOI), editor Peter deMenocal and three anonymous reviewers for constructive reviews and discussion. Cruise NBP0805 was funded by NSF Office of Polar Programs (OPP) Antarctic Sciences (grant number ANT-0636787). Data from the Palmer LTER data archive were supported by Office of Polar Programs, NSF grants OPP-9011927, OPP-9632763 and OPP-0217282. The work was funded by the Natural Environment Research Council (NERC) grant NE/F005296/1 and an Antarctic Science Bursary. The authors declare no competing financial interests.

Correspondence and requests for materials should be addressed to K.R.H. (e-mail: kathh@earth.ox.ac.uk).

Figure 1: A) Location of sample sites in the Southern Ocean and coastal Antarctica. Grey stars indicate modern sponge sample sites; grey squares indicate deep-water samples; grey dotted circles show cores PC034 and KC081. Map production by K. Scanlon (USGS).

B) Dissolved silicic acid concentrations from across the Drake Passage. Drawn using Ocean Data View (Schlitzer, 2000).

Figure 2: A) The relationship between modern sponge silicon isotope composition and ambient seawater $Si(OH)_4$ concentration (r^2=0.75; Equation 2). Filled symbols show values for Hexactinellid sponges; open symbols show values for Demosponges. There is no consistent difference between the two classes of sponges, although there may be species-specific fractionation (~0.5‰). Error bars show $2\sigma_{SD}$.

B) Isotopic homogeneity between individuals of the same species from one locality, and within an individual. The black symbols show duplicate measurements of spicule silicon isotopes taken from three different specimens; the white triangles show the silicon isotopic composition of two specimens of *Rosella* collected from the same site; the white circles show the silicon isotopic composition of two different types of spicules from the same specimen (dermal and perenchymal). Error bars show $2\sigma_{SD}$.

656 C) A three-isotope plot for all sponge samples. The equation was calculated using
657 model II regression, and numbers in parentheses indicate 95% confidence
658 intervals of the slope and intercept respectively. The relationship between
659 $\delta^{29}Si_{sponge}$ and $\delta^{30}Si_{sponge}$ is consistent with mass dependent fractionation under
660 kinetic equilibrium. Error bars show $2\sigma_{SD}$.

661 Figure 3: Fractionation of silicon isotopes by sponges. The black circles show the
662 fractionation by sponges from the deep Southern Ocean; the grey squares show
663 the fractionation by sponges from the West Antarctic Peninsula; the white triangles
664 show the fractionation by sponges from the deep North Atlantic (assuming Atlantic
665 deep water $\delta^{30}Si_{Si(OH)4}$ = 1.6‰; Reynolds, 2009). Fractionation is plotted against
666 ambient A) Si(OH)4 concentrations; B) salinity; C) temperature and D) pH (data
667 from the British Antarctic Survey and Garcia et al., 2006). Error bars are
668 propagated from $\pm 2\sigma_{SD}$ of $\delta^{30}Si_{Si(OH)4}$ and $\delta^{30}Si_{sponge}$.

669 Figure 4: A) Age models for the two cores based on magnetic susceptibility
670 (dashed lines) and diatom abundances (squares). Note for PC034, the shallower
671 peak in magnetic susceptibility has been interpreted as showing the Antarctic
672 Climate Reversal. For KC081, age constraints are also available from the
673 occurrence of the radiolarian *Cycladophora davisiana* (triangles), which are
674 abundant in glacial sediments, and corrected radiocarbon ages (indicated by black
675 arrows) showing core top ~ 6.3 ka, 0.23 mbsf ~ 11.3 ka and 1.59 mbsf ~ 23.5 ka
676 (NERC Publication Code AA-28113-5). Data and interpretation from C. Allen
677 (BAS). Also shown are locations of the cores with respect to major oceanographic
678 fronts, although these can vary by several degrees in the modern setting (SAF =
679 Sub-Antarctic Front; PF = Polar Front; SACCF = Southern Antarctic Circumpolar
680 Front; SB = Southern Boundary of the ACC, adapted from Naveira Garabato et al.,
681 2002). White symbols correspond to the northern core (KC081) and black
682 symbols to the southern core (PC034).

683 B) Composition of sponges (error bars show $2\sigma_{SD}$) and reconstructed deep-water
684 $Si(OH)_4$ concentrations (95% confidence intervals ~ 20 μM; Equation 2). White
685 symbols correspond to the northern core (KC081) and black symbols to the
686 southern core (PC034). The white box shows $\delta^{30}Si$ of modern sponges found near
687 KC081; the black box shows $\delta^{30}Si$ of modern sponges found near PC034. The
688 age model is based on the information in A). Also shown: opal flux and
689 $^{231}Pa/^{230}Th$ from core TN057-13-4PC from south of the Polar Front in the Atlantic
690 Sector (Anderson et al., 2009); EPICA ice core records of pCO_2 and δD, a proxy
691 for local temperature (Indermüle et al., 1999; Fluckiger et al., 1999; Monnin et al.,
692 2001, 2004).

693

694

Sample code	Classification	Location	Depth (m)	Method	Lat (°S)	Lon (°W)
NBP0805-TB1-3	Unidentified Demosponge	Burdwood Bank	306-333	Blake trawl	54.48	62.18
NBP0805-TB1-6	Mycalidae	Burdwood Bank	306-333	Blake trawl	54.48	62.18
NBP0805-TB1-11	Unidentified Hexactinellid	Burdwood Bank	306-333	Blake trawl	54.48	62.18
NBP0805-TB3-21	Mycalidae	Burdwood Bank	2215-2343	Blake trawl	54.91	62.03
NBP0805-TB4-3	Unidentified Demosponge	Burdwood Bank	804-828	Blake trawl	54.74	62.21
NBP0805-TB4-24	Unidentified Demosponge	Burdwood Bank	804-828	Blake trawl	54.74	62.21
NBP0805-TB4-27	*Rosella*	Burdwood Bank	804-828	Blake trawl	54.74	62.21
NBP0805-TO1-27	*Rosella*	Elephant Island	407-428	Otter trawl	61.25	56.42
NBP0805-TO1-57	*Rosella*	Elephant Island	407-428	Otter trawl	61.25	56.42
NBP0805-TO3-100	Unidentified Demosponge	Drake Passage	689-914	Otter trawl	60.56	65.97
NBP0805-TO3-111	Unidentified Demosponge	Drake Passage	689-914	Otter trawl	60.56	65.97
NBP0805-DR7-47	*Acoelocalyx*	Scotia Sea	2109-2422	Dredge	54.88	40.69
NBP0805-DR13-47	*Acoelocalyx*	Scotia Sea	2097-2477	Dredge	59.50	42.50
NBP0805-DR16-47	*Acoelocalyx*	Scotia Sea	930-	Dredge	61.10	56.45

NBP0805-DR29-47	*Acoelocalyx*	Drake Passage	1070 758-759	Dredge	60.56	65.91
NBP0805-DR34-47	*Acoelocalyx*	Drake Passage	899-838	Dredge	59.73	68.74
NBP0805-DR35-111	Unidentified Demosponge	Drake Passage	672-718	Dredge	59.72	68.88
NBP0805-DR40-47	*Acoelocalyx*	Drake Passage	1294-1351	Dredge	59.73	68.93
CRS-956	Unidentified Demosponge	Anvers Island	600	Dredge	64.78	65.30
RB-Mycale	*Mycale*	Adelaide Island	10	Hand collection	67.57	68.23

695

696 Table 1: Samples used in the modern calibration collected from the Southern
697 Ocean. CRS-956 was collected by R. Waller (University of Hawaii) from near
698 Anvers Island; RB-Mycale was collected by J. Berman (BAS) from near Adelaide
699 Island.

Core	Depth (m)	Latitude (°S)	Longitude (°W)
PC034	1652	59.79	39.60
KC081	3662	56.74	42.97

700

701 Table 2: Locations of cores used in this study.

702

Sample code	T (˚C)	S (psu)	pH	$Si(OH)_4$ (μM)	$\delta^{30}Si$ (‰)	$\delta^{29}Si$ (‰)	$*\delta^{30}Si$ (‰)
NBP0805-TB1-3	4.3	34.17	7.96	12	-0.70(0.04)	-0.38(0.02)	-0.36
NBP0805-TB1-6	4.3	34.17	7.96	12	-1.01(0.08)	-0.51(0.05)	-0.52

Repeat dissolution					-1.15 (0.04)	-0.61 (0.03)	-0.59
NBP0805-TB1-11	4.3	34.17	7.96	12	-1.69(0.03)	-0.84(0.03)	-0.86
NBP0805-TB3-21	1.8	34.69	7.70	97	-2.79(0.02)	-1.45(0.02)	-1.42
NBP0805-TB4-3	3.1	34.35	7.80	56	-1.55(0.03)	-0.83(0.02)	-0.79
NBP0805-TB4-24	3.1	34.35	7.80	56			
Dermal					-2.87(0.04)	-1.41(0.02)	-1.46
Perenchymal					-2.96(0.04)	-1.51(0.01)	-1.51
NBP0805-TB4-27	3.1	34.35	7.80	56	-2.54(0.04)	-1.28(0.02)	-1.30
NBP0805-TO1-27	1.9	34.65	7.71	90	-3.83(0.05)	-1.94(0.02)	-1.95
NBP0805-TO1-57	1.9	34.65	7.71	90	-3.51(0.04)	-1.83(0.02)	-1.79
NBP0805-TO3-100	2.4	34.63	7.80	75	-3.06(0.04)	-1.59(0.02)	-1.56
NBP0805-TO3-111	2.4	34.63	7.80	75	-2.88(0.09)	-1.46(0.06)	-1.47
Repeat dissolution					-3.18 (0.05)	-1.64 (0.03)	-1.62
NBP0805-DR7-47	1.5	35	7.7	120	-3.76(0.05)	-1.92(0.05)	-1.92
					-3.58(0.02)	-1.77(0.03)	-1.82
NBP0805-DR13-47	1.5	35	7.7	110	-3.20(0.05)	-1.59(0.02)	-1.63
NBP0805-DR16-47	1.48	34.72	7.76	96	-4.13(0.05)	-2.10(0.04)	-2.10
NBP0805-DR29-47	2.4	34.63	7.80	100	-3.91(0.04)	-2.02(0.01)	-1.99
					-3.91(0.05)	-2.02(0.02)	-1.99
NBP0805-DR34-47	2.3	34.62	7.80	75	-2.54(0.03)	-1.31(0.02)	-1.30
NBP0805-DR35-111	2.4	34.64	7.80	70	-2.86(0.04)	-1.44(0.03)	-1.46
NBP0805-DR40-47	1.9	34.70	7.72	94	-2.92(0.03)	-1.47(0.01)	-1.49
CRS-956	1.5	34.72		107	-3.36(0.04)	-1.72(0.02)	-1.71

RB-Mycale Repeat dissolution	-0.4	33	8.19	50	-2.39(0.05) -2.34(0.03) -2.40(0.03)	-1.21(0.03) -1.21(0.02) -1.24(0.03)	-1.22 -1.19 -1.22

703

704 Table 3: Silicon isotopic composition of modern sponge spicules. Temperature,
705 salinity, pH and nutrient values courtesy of WHOI, BAS, Palmer LTER, WOCE
706 (Schlitzer, 2000) and World Ocean Atlas 05 (WOA05; Garcia et al., 2006).
707 Numbers in parentheses are 2($\sigma/\sqrt{n}$). *δ^{30}Si is the expected δ^{29}Si value calculated
708 assuming mass dependent fractionation:

709 $$*\delta^{30}Si = 0.51 \times \delta^{30}Si_{sponge}$$

Sample	Lat (°S)	Long (°W)	Depth (m)	Si(OH)4	δ^{30}Si
CTD2-1-1	54.88	62.14	2190	96.5	1.06 (0.04)
CTD2-13-7	54.88	62.14	805	56.0	1.28 (0.03)
CTD2-17-9	54.88	62.14	300	11.8	1.76 (0.05)
CAM3-bottom	61.28	56.42	400	95.8	1.03 (0.05)
CAM7-1500	60.55	65.94	1500	100.6	1.10 (0.06)
repeat					1.04 (0.06)
CAM8-600	59.89	68.86	600	40.4	1.40 (0.06)

710

711 Table 4: Seawater $Si(OH)_4$ and δ^{30}Si values. $Si(OH)_4$ measured by WHOI nutrient
712 facility; δ^{30}Si measured using a co-precipitation method. Numbers in parentheses
713 are 2($\sigma/\sqrt{n}$).

714

Figure

Click here to download high resolution image

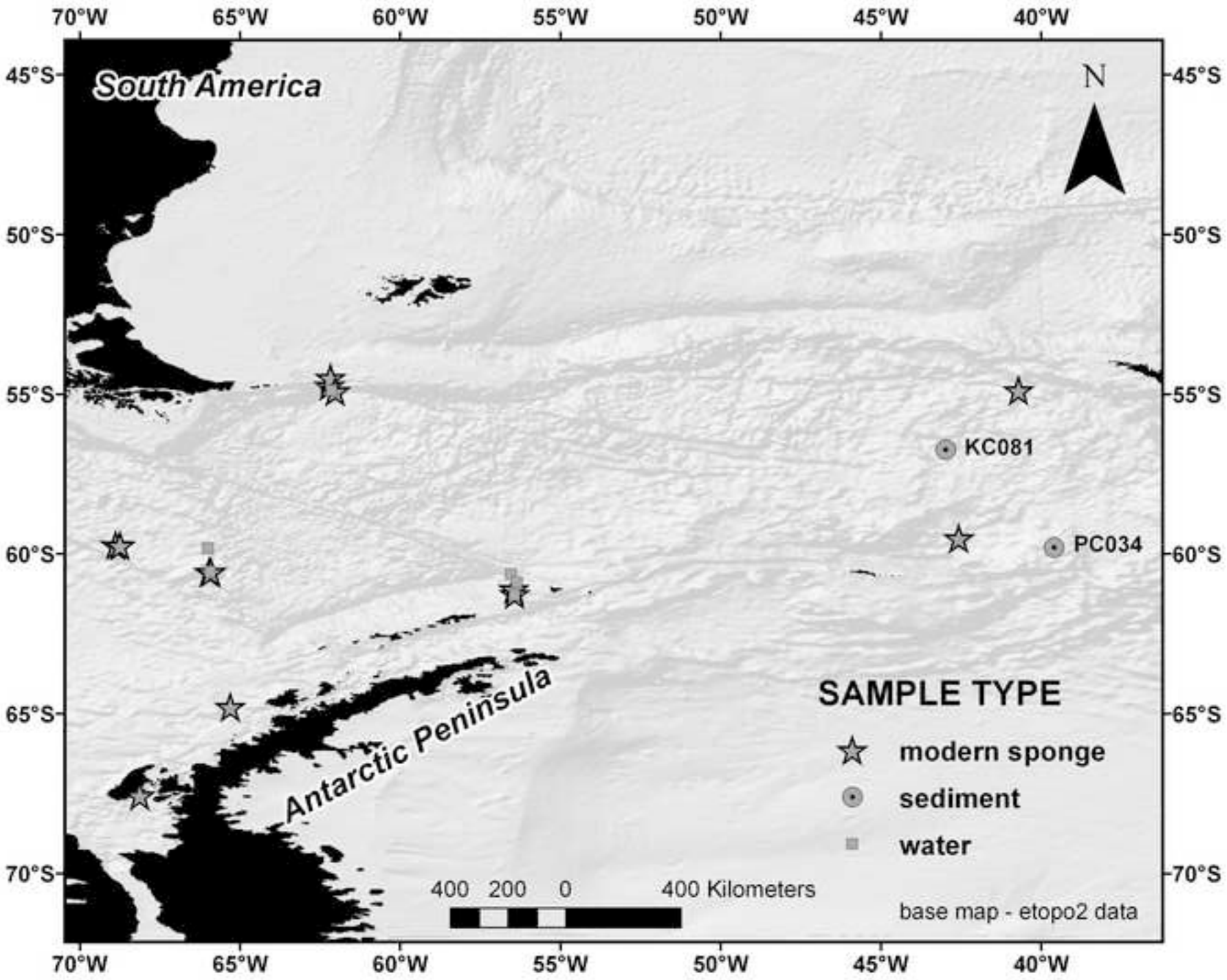

Figure

Click here to download high resolution image

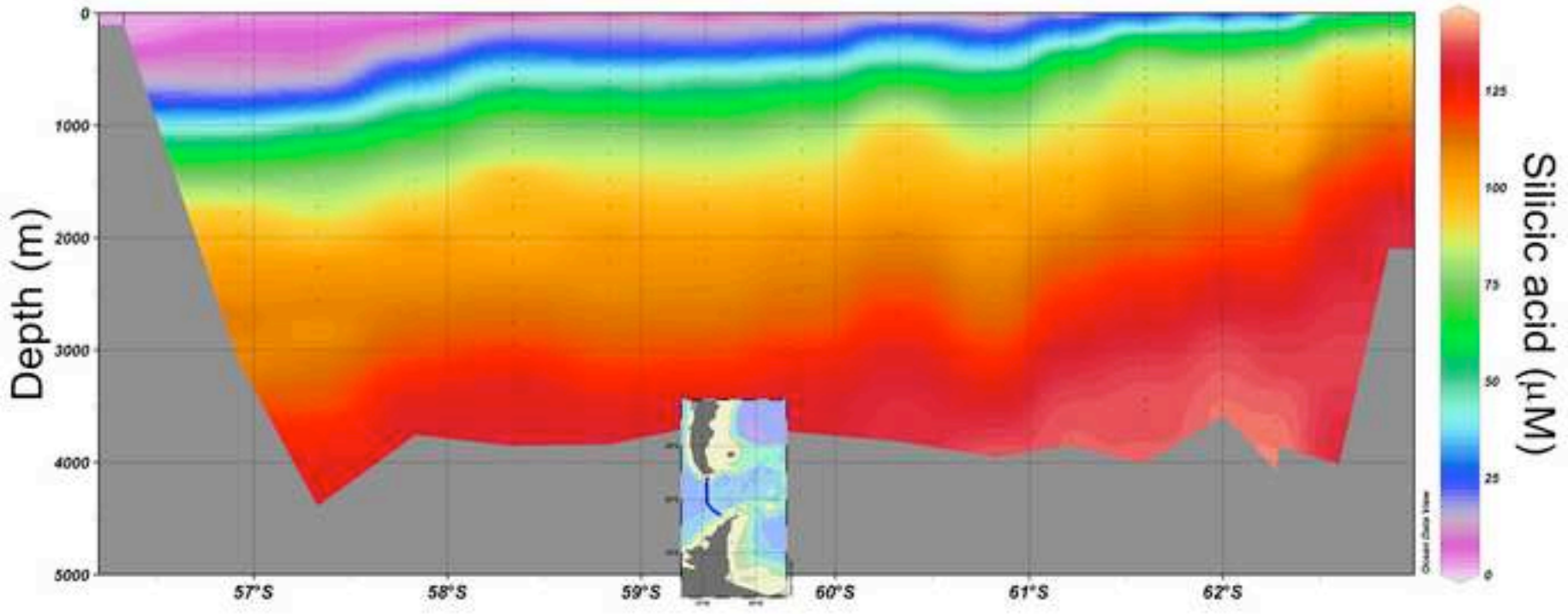

Figure
Click here to download high resolution image

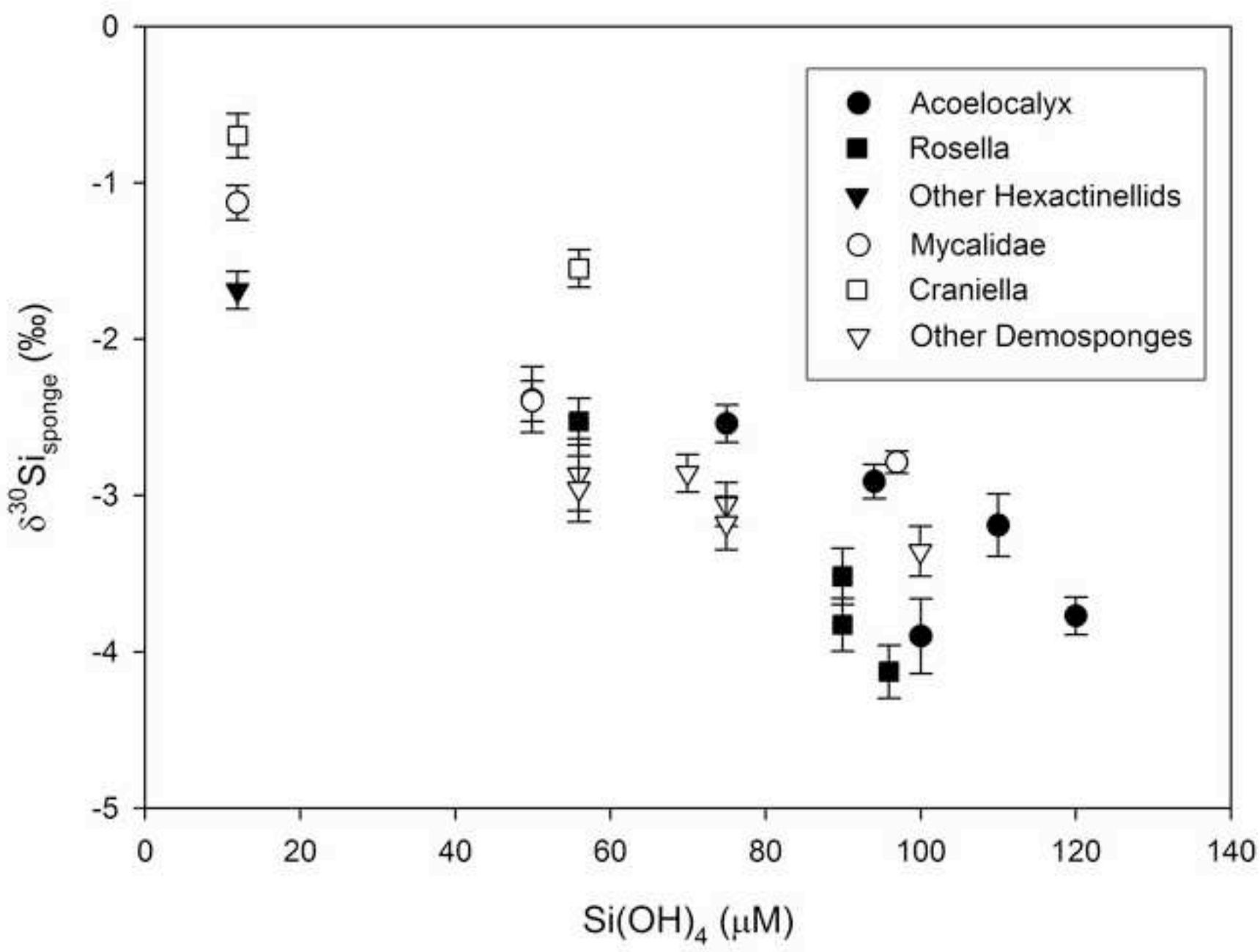

Figure
Click here to download high resolution image

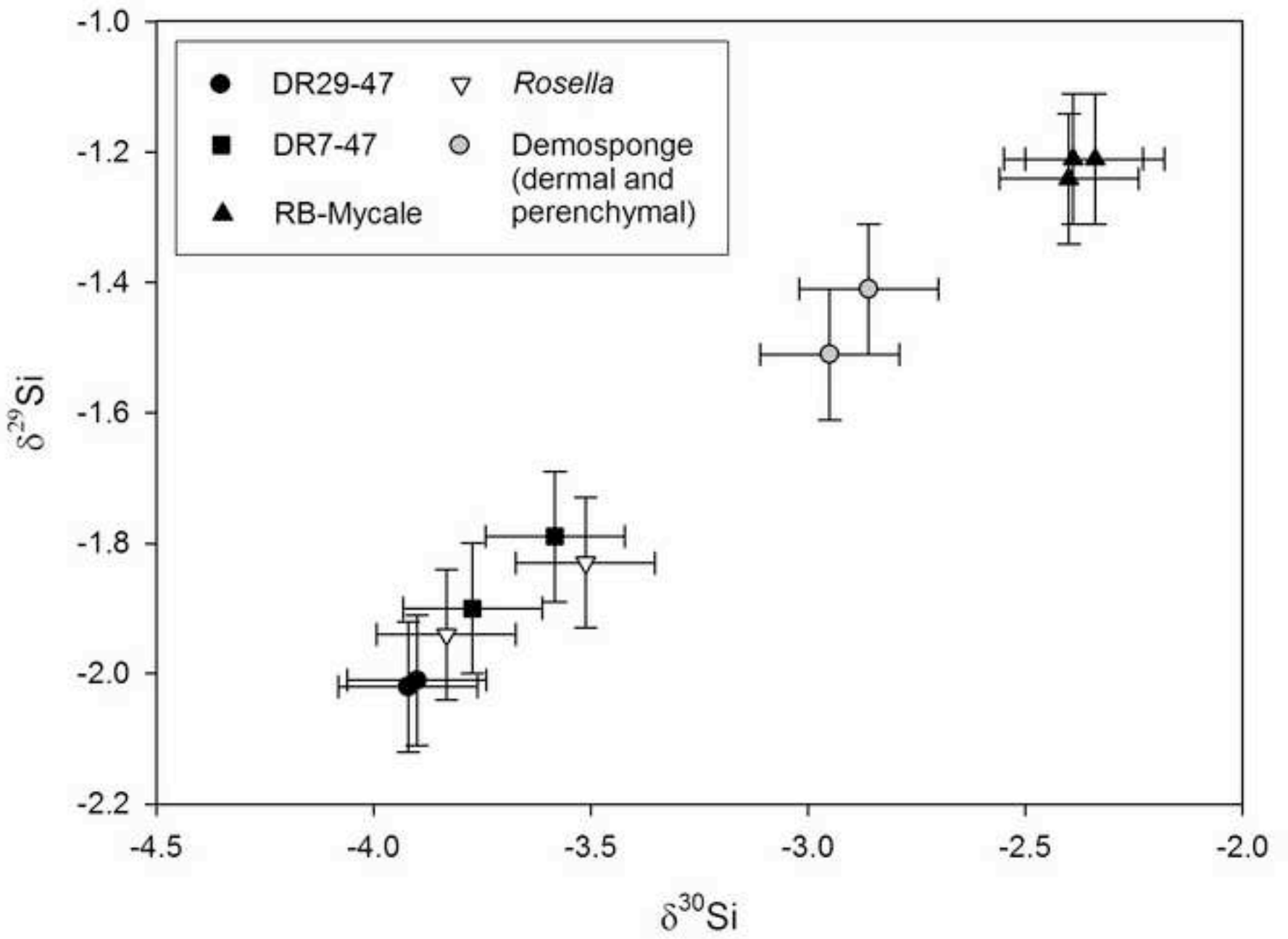

Figure
Click here to download high resolution image

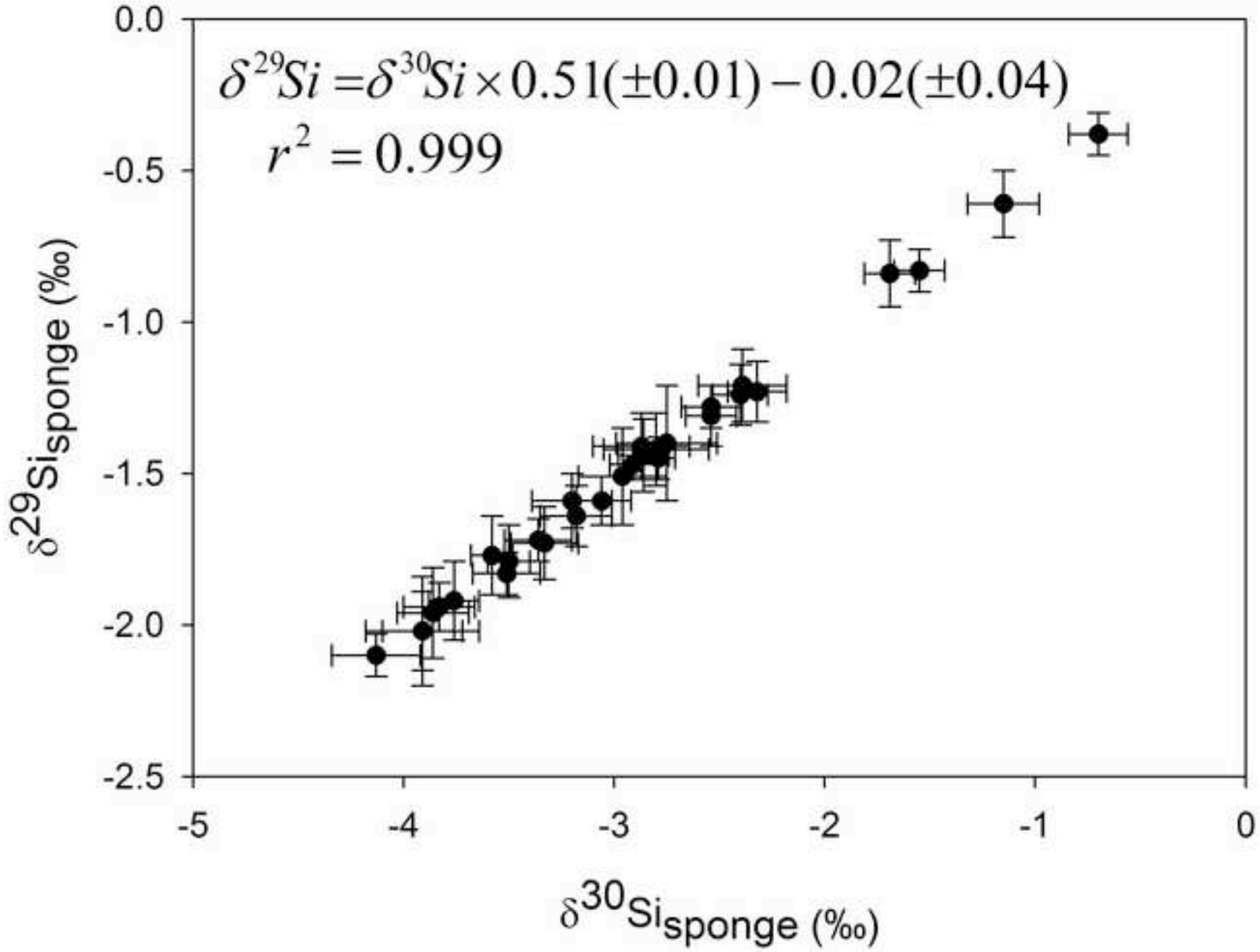

Figure

Click here to download high resolution image

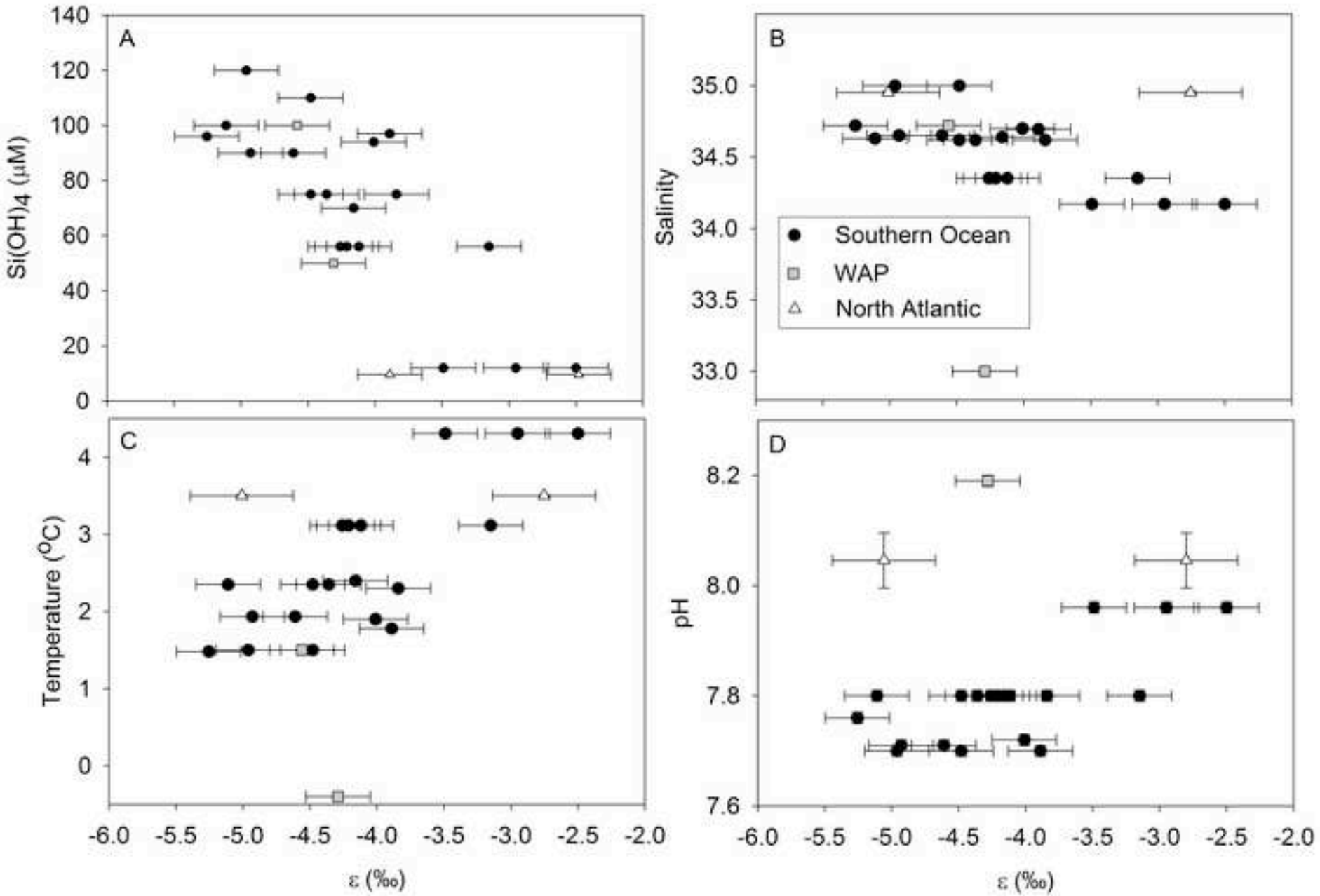

Figure

Click here to download high resolution image

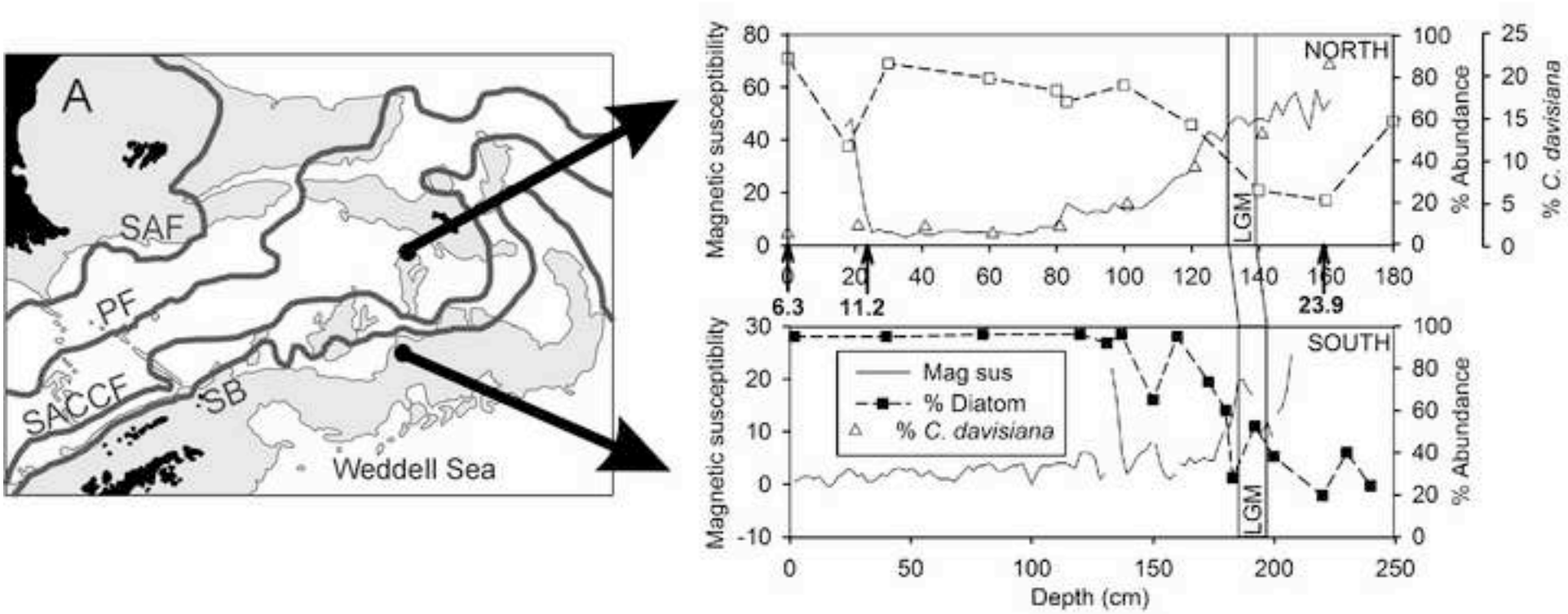

Figure

Click here to download high resolution image